Nonrelativistic quark model analysis of T_{cc}

Sungsik Noh[*] and Woosung Park[†]

Department of Physics and Institute of Physics and Applied Physics, Yonsei University, Seoul 03722, Korea

(Received 8 March 2023; accepted 15 June 2023; published 7 July 2023)

The recent discovery of the doubly charmed tetraquark T_{cc} ($\bar{u}\,\bar{d}\,cc$) provides a stringent constraint on its binding energy relative to its lowest decay threshold. We use a fully convergent spatial wave function and perform a simultaneous global fit to both the meson and baryon spectra. Our analysis shows that a Yukawa type hyperfine potential leads to a slight bound state for T_{cc} with $(I, S) = (0, 1)$ below its lowest threshold, in agreement with recent experimental findings. We also find that T_{cc} is highly likely to be in a compact configuration.

DOI: 10.1103/PhysRevD.108.014004

I. INTRODUCTION

There is a renewed excitement in hadron physics over the observations of numerous exotic hadron candidates [1–5]. Of particular interest is the recently observed flavor exotic T_{cc} state, which is an explicit four quark state. T_{cc} was first predicted in Refs. [6,7] based on the strong color-spin attraction of $\bar{u}\,\bar{d}$ quark pair that can bind the tetraquark configuration. Many quark model calculations for T_{cc} followed [8–30], which unfortunately varied on the predicted masses and even on whether the mass lies above or below the lowest threshold. Therefore, the recent observation of T_{cc} [1] provides a good opportunity where all the models can be tested in a hitherto untested multiquark configuration, thereby leading us to identify the correct model to describe the low energy confinement phenomena of quantum chromodynamcis (QCD).

Accurate model calculations are a crucial requirement for fully testing a quark model and refining our understanding of the underlying physics that governs the behavior of quarks and the strong force. However, these calculations required to accurately model the behavior of quarks in such a system are extremely difficult. To perform such an exact calculation, one has to introduce a complete set of spatial wave functions, which necessarily contain all possible internal states. Also, a simultaneous global fit to both the meson and baryon spectra should be performed in the model calculations. However, only a few works satisfy these requirements among the works mentioned above [6–30]. Furthermore, no work could correctly predict both the mass and binding energy of T_{cc} simultaneously. For example, in our latest publication [30], we successfully predicted the mass of T_{cc} using a Gaussian type hyperfine potential, whereas the binding energy was obtained to be higher than the experimental measurement by 13 MeV.

The hyperfine potential strongly affects the binding energy of the multiquark configuration, with the strong color-spin attraction coming from the $\bar{u}\,\bar{d}$ quark pair. We thus analyze the effect of a Yukawa type hyperfine potential on the binding energy in comparison with the Gaussian type hyperfine potential. Our analysis suggests that a Yukawa type hyperfine potential is necessary to accurately reproduce the experimentally observed slight binding of T_{cc}, rather than a Gaussian type.

On the other hand, the heavy quark component of T_{cc} is made up of open charm quarks, while that of $X(3872)$ is composed of hidden charm quarks. The fact that there have been no satisfactory explanations for the internal structure of the X(3872) in the two decades since its experimental discovery sharply illustrates the lack of understanding of quark interactions in the quark model, as well as the complexity of tetraquark structures. In this paper, we propose the possibility of a compact and bound structure for T_{cc}, based on a deep comprehension of the interaction of the $\bar{u}\,\bar{d}$ pair. This may provide a clue to solving the burning issue of the $X(3872)$ with another residual strong force and lead to a more in-depth theoretical approach to multiquark structures beyond the tetraquark.

Among the researches for the T_{cc}, there are chiral quark models based on color-flavor interaction. However, those model studies predicted bindings that are too strong in the T_{cc} channel [11,13,15,17,18,26]. Thus, any modification should start from the gluon exchange quark models.

[*]sungsiknoh@yonsei.ac.kr
[†]diracdelta@yonsei.ac.kr

II. MODEL DESCRIPTION

In our nonrelativisitc quark model, we solve the Schrödinger equation with the Hamiltonian given as follows.

$$H = \sum_{i=1}^{4}\left(m_i + \frac{\mathbf{p}_i^2}{2m_i}\right) - \frac{3}{4}\sum_{i<j}^{4}\frac{\lambda_i^c}{2}\frac{\lambda_j^c}{2}(V_{ij}^C + V_{ij}^{CS}), \quad (1)$$

where m_i is the quark mass for the ith quark and $\lambda_i^c/2$ is the SU(3) color operator. The confinement potential V_{ij}^C is identical to that used in previous studies [15,17,30], given as follows.

$$V_{ij}^C = -\frac{\kappa}{r_{ij}} + \frac{r_{ij}}{a_0^2} - D, \quad (2)$$

However, for the hyperfine potential V_{ij}^{CS}, we introduce a Yukawa type potential given by

$$V_{ij}^{CS} = \frac{\hbar^2 c^2 \kappa'}{m_i m_j c^4}\frac{e^{-r_{ij}/r_{0ij}}}{(r_{0ij})r_{ij}}\boldsymbol{\sigma}_i \cdot \boldsymbol{\sigma}_j, \quad (3)$$

where $\boldsymbol{\sigma}_i$ is the SU(2) spin operator and $r_{ij} \equiv |\mathbf{r}_i - \mathbf{r}_j|$ is the relative distance between the i and j quarks. In addition, κ' and r_{0ij} depend on the masses of quark pair as given in Ref. [30]:

$$r_{0ij} = 1/\left(\alpha + \beta\frac{m_i m_j}{m_i + m_j}\right), \quad (4)$$

$$\kappa' = \kappa_0\left(1 + \gamma\frac{m_i m_j}{m_i + m_j}\right). \quad (5)$$

Our Yukawa type potential in Eq. (3) satisfies the contact term $\delta(r_{ij})$ in the heavy quark limit as r_{ij} approaches zero. The model parameters in the Hamiltonian in Eq. (1) are determined by fitting them to a total of 33 ground state hadron masses listed in Tables I and II. Further, we obtain an optimized set of model parameters in such a way that χ^2 value of the Pearson's chi-squared test formula should be minimized. The model parameters selected for this study are as follows.

$$\begin{aligned}
&\kappa = 97.7\ \text{MeV fm}, && a_0 = 0.0327338\ (\text{MeV}^{-1}\ \text{fm})^{1/2},\\
&D = 959\ \text{MeV},\\
&m_u = 315\ \text{MeV}, && m_s = 610\ \text{MeV},\\
&m_c = 1895\ \text{MeV}, && m_b = 5274\ \text{MeV},\\
&\alpha = 1.1349\ \text{fm}^{-1}, && \beta = 0.0011554\ (\text{MeV fm})^{-1},\\
&\gamma = 0.001370\ \text{MeV}^{-1}, && \kappa_0 = 213.244\ \text{MeV}. \quad (6)
\end{aligned}$$

TABLE I. This table shows the masses of mesons obtained (Column 3) from the model calculation in this work with the fitting parameters set given in Eq. (6). Column 4 shows the variational parameter a.

Particle	Experimental value (MeV)	Mass (MeV)	Variational parameter (fm^{-2})
D	1864.8	1865.0	$a = 6.8$
D^*	2007.0	2009.4	$a = 5.1$
η_c	2983.6	3008.2	$a = 22.4$
J/Ψ	3096.9	3131.2	$a = 17.0$
D_s	1968.3	1967.0	$a = 11.0$
D_s^*	2112.1	2103.5	$a = 5.1$
K	493.68	497.17	$a = 7.2$
K^*	891.66	872.74	$a = 3.6$
B	5279.3	5276.3	$a = 6.5$
B^*	5325.2	5331.8	$a = 5.8$
η_b	9398.0	9368.6	$a = 78.9$
Υ	9460.3	9485.0	$a = 61.6$
B_s	5366.8	5345.6	$a = 11.5$
B_s^*	5415.4	5404.8	$a = 10.1$
B_c	6275.6	6276.2	$a = 32.7$
B_c^*	...	6361.8	$a = 26.9$

TABLE II. Same as Table I but for baryons. In column 4, a_1 and a_2 are the variational parameters.

Particle	Experimental value (MeV)	Mass (MeV)	Variational parameters (fm^{-2})
Λ	1115.7	1105.1	$a_1 = 4.0$, $a_2 = 3.2$
Λ_c	2286.5	2268.3	$a_1 = 4.2$, $a_2 = 3.8$
Ξ_{cc}	3621.4	3623.8	$a_1 = 10.2$, $a_2 = 4.1$
Λ_b	5619.4	5600.8	$a_1 = 4.3$, $a_2 = 4.2$
Σ_c	2452.9	2448.2	$a_1 = 2.6$, $a_2 = 5.1$
Σ_c^*	2517.5	2530.6	$a_1 = 2.3$, $a_2 = 4.4$
Σ_b	5811.3	5817.3	$a_1 = 2.5$, $a_2 = 5.4$
Σ_b^*	5832.1	5849.4	$a_1 = 2.4$, $a_2 = 5.1$
Σ	1192.6	1193.6	$a_1 = 2.7$, $a_2 = 4.5$
Σ^*	1383.7	1400.8	$a_1 = 2.0$, $a_2 = 3.0$
Ξ	1314.9	1314.3	$a_1 = 4.1$, $a_2 = 4.1$
Ξ^*	1531.8	1530.4	$a_1 = 3.8$, $a_2 = 2.5$
Ξ_c	2467.8	2465.4	$a_1 = 4.6$, $a_2 = 5.4$
Ξ_c^*	2645.9	2642.8	$a_1 = 2.9$, $a_2 = 5.7$
Ξ_b	5787.8	5785.7	$a_1 = 4.7$, $a_2 = 6.3$
Ξ_b^*	5945.5	5950.2	$a_1 = 3.1$, $a_2 = 6.9$
p	938.27	941.58	$a_1 = 2.6$, $a_2 = 2.6$
Δ	1232	1262.8	$a_1 = 1.7$, $a_2 = 1.7$

We utilize the same methods as in Ref. [30] to construct the wave function and calculate the masses of tetraquarks as well as those of mesons and baryons. To solve the Hamiltonian, we set the Jacobi coordinates for the tetraquark configuration in the center of mass frame as follows.

(i) Coordinate set 1

$$\mathbf{x}_1 = \frac{1}{\sqrt{2}}(\mathbf{r}_1 - \mathbf{r}_2), \qquad \mathbf{x}_2 = \frac{1}{\sqrt{2}}(\mathbf{r}_3 - \mathbf{r}_4),$$
$$\mathbf{x}_3 = \frac{1}{\mu}\left(\frac{m_1\mathbf{r}_1 + m_2\mathbf{r}_2}{m_1 + m_2} - \frac{m_3\mathbf{r}_3 + m_4\mathbf{r}_4}{m_3 + m_4}\right), \tag{7}$$

(ii) Coordinate set 2

$$\mathbf{y}_1 = \frac{1}{\sqrt{2}}(\mathbf{r}_1 - \mathbf{r}_3), \qquad \mathbf{y}_2 = \frac{1}{\sqrt{2}}(\mathbf{r}_4 - \mathbf{r}_2),$$
$$\mathbf{y}_3 = \frac{1}{\mu}\left(\frac{m_1\mathbf{r}_1 + m_2\mathbf{r}_3}{m_1 + m_2} - \frac{m_3\mathbf{r}_2 + m_4\mathbf{r}_4}{m_3 + m_4}\right), \tag{8}$$

(iii) Coordinate set 3

$$\mathbf{z}_1 = \frac{1}{\sqrt{2}}(\mathbf{r}_1 - \mathbf{r}_4), \qquad \mathbf{z}_2 = \frac{1}{\sqrt{2}}(\mathbf{r}_2 - \mathbf{r}_3),$$
$$\mathbf{z}_3 = \frac{1}{\mu}\left(\frac{m_1\mathbf{r}_1 + m_2\mathbf{r}_4}{m_1 + m_2} - \frac{m_3\mathbf{r}_2 + m_4\mathbf{r}_3}{m_3 + m_4}\right), \tag{9}$$

where

$$\mu = \left[\frac{m_1^2 + m_2^2}{(m_1 + m_2)^2} + \frac{m_3^2 + m_4^2}{(m_3 + m_4)^2}\right]^{1/2},$$

and

$$\begin{aligned}
&m_u = m_d;\\
&m_1 = m_2 = m_u, \quad m_3 = m_4 = m_c \quad \text{for } \bar{u}\,\bar{d}\,cc,\\
&m_1 = m_2 = m_u, \quad m_3 = m_4 = m_b \quad \text{for } \bar{u}\,\bar{d}\,bb,\\
&m_1 = m_2 = m_u, \quad m_3 = m_c, m_4 = m_b \quad \text{for } \bar{u}\,\bar{d}\,cb.
\end{aligned}$$

For the tetraquark configuration with the isospin $I = 0$, which is in the S-wave state, the wave function of the Hamiltonian is constructed by combining the spatial wave function with the color-spin basis, satisfying the symmetry properties imposed by the Pauli principle. The detailed description for the color-spin part of the wave function are given in Sec. III of Ref. [30]. We construct the spatial wave function of the tetraquark through the three independent harmonic oscillator bases corresponding to each Jacobi coordinate. In particular, the spatial wave function is characterized by the quanta Q, which can be defined by the internal quantum numbers corresponding to each Jacobi coordinate as in our previous work [30].

$$Q = 2n_1 + 2n_2 + 2n_3 + l_1 + l_2 + l_3. \tag{10}$$

We use a complete set of harmonic oscillator bases up to the 5th quanta ($Q = 8$) to the spatial part of wave functions. The following are a few examples of spatial bases in the S-wave state, denoted as $\psi^{\text{spatial}}_{[n_1,n_2,n_3,l_1,l_2,l_3]}$, which belong to each quanta.

$$\begin{aligned}
\psi^{\text{spatial}}_{[0,0,0,0,0,0]} &= \left(\frac{2}{\pi}\right)^{\frac{9}{4}} a_1^{\frac{3}{4}} a_2^{\frac{3}{4}} a_3^{\frac{3}{4}} \exp[-a_1\mathbf{x}_1^2 - a_2\mathbf{x}_2^2 - a_3\mathbf{x}_3^2],\\
\psi^{\text{spatial}}_{[0,0,0,1,1,0]} &= -\frac{4}{\sqrt{3}}\left(\frac{2}{\pi}\right)^{\frac{9}{4}} a_1^{\frac{5}{4}} a_2^{\frac{5}{4}} a_3^{\frac{3}{4}} \mathbf{x}_1\cdot\mathbf{x}_2 \exp[-a_1\mathbf{x}_1^2 - a_2\mathbf{x}_2^2 - a_3\mathbf{x}_3^2],\\
\psi^{\text{spatial}}_{[0,0,0,2,2,0]} &= -\frac{8}{3\sqrt{5}}\left(\frac{2}{\pi}\right)^{\frac{9}{4}} a_1^{\frac{7}{4}} a_2^{\frac{7}{4}} a_3^{\frac{3}{4}} \left[\mathbf{x}_1^2\mathbf{x}_2^2 - 3(\mathbf{x}_1\cdot\mathbf{x}_2)^2\right] \exp[-a_1\mathbf{x}_1^2 - a_2\mathbf{x}_2^2 - a_3\mathbf{x}_3^2],\\
\psi^{\text{spatial}}_{[0,0,0,1,2,3]} &= \frac{32}{15\sqrt{21}}\left(\frac{2}{\pi}\right)^{\frac{9}{4}} a_1^{\frac{5}{4}} a_2^{\frac{7}{4}} a_3^{\frac{9}{4}} \left[6\mathbf{x}_3^2(\mathbf{x}_1\cdot\mathbf{x}_2)(\mathbf{x}_2\cdot\mathbf{x}_3) + 3(\mathbf{x}_1\cdot\mathbf{x}_3)(\mathbf{x}_2^2\mathbf{x}_3^2 - 5(\mathbf{x}_2\cdot\mathbf{x}_3)^2)\right] \exp[-a_1\mathbf{x}_1^2 - a_2\mathbf{x}_2^2 - a_3\mathbf{x}_3^2],\\
\psi^{\text{spatial}}_{[0,0,0,2,2,4]} &= \frac{32\sqrt{2}}{105\sqrt{3}}\left(\frac{2}{\pi}\right)^{\frac{9}{4}} a_1^{\frac{7}{4}} a_2^{\frac{7}{4}} a_3^{\frac{11}{4}} \left[\mathbf{x}_1^2\mathbf{x}_2^2\mathbf{x}_3^4 + 2\mathbf{x}_3^4(\mathbf{x}_1\cdot\mathbf{x}_2)^2 - 20\mathbf{x}_3^2(\mathbf{x}_1\cdot\mathbf{x}_2)(\mathbf{x}_1\cdot\mathbf{x}_3)(\mathbf{x}_2\cdot\mathbf{x}_3) + 35(\mathbf{x}_1\cdot\mathbf{x}_3)^2(\mathbf{x}_2\cdot\mathbf{x}_3)^2\right.\\
&\quad \left. - 5(\mathbf{x}_2^2\mathbf{x}_3^2(\mathbf{x}_1\cdot\mathbf{x}_3)^2 + \mathbf{x}_1^2\mathbf{x}_3^2(\mathbf{x}_2\cdot\mathbf{x}_3)^2)\right] \exp[-a_1\mathbf{x}_1^2 - a_2\mathbf{x}_2^2 - a_3\mathbf{x}_3^2].
\end{aligned} \tag{11}$$

The parameters a_1, a_2, and a_3 appearing in Eq. (11) are determined through the variational method in such a way that it gives a minimum to the diagonalized Hamiltonian matrix elements in terms of all the spatial wave functions up to the 5th quanta of bases. The variational parameters for the masses of mesons and baryons listed in Tables I and II are also determined in this way. This makes it all the more possible that the tetraquark configurations should have an exact solution to the Hamiltonian.

III. NUMERICAL RESULTS

The results of our calculations for $T_{cc}(\bar{u}\,\bar{d}\,cc)$, $T_{cb}(\bar{u}\,\bar{d}\,cb)$, and $T_{bb}(\bar{u}\,\bar{d}\,bb)$ using our Yukawa type hyperfine potential are presented in Table III. Comparing the present results for T_{cc} with those from our previous publication [30] where used a Gaussian type hyperfine potential, we find that both models reproduce the mass well. However, our previous calculation predicted an unbound T_{cc} state, while our current model indicates that it lies slightly below the threshold consistent with the experimental observations. This suggests that the Yukawa type hyperfine potential used in our current calculation may better capture the strong interaction dynamics of the T_{cc} configuration. Further research is necessary to fully understand the implications of our findings. Our present model using a Yukawa type hyperfine potential also shows significantly stronger binding energies for T_{cc} and T_{cb} than the model with a Gaussian type hyperfine potential presented in Ref. [30].

The discovery of T_{cc} is of great significance since it allows for testing the validity of quark models. In this regard, we compare our present results with those from Refs. [15,17,30] in Table III. The results from those quark models were also calculated with a complete set of spatial wave functions, but obtained using different forms of Gaussian or Yukawa type of hyperfine potential. Specifically, Ref. [30] used a Gaussian type hyperfine potential, while Refs. [15,17], including our present work, used a Yukawa type of hyperfine potential.

Comparing the results in this work with those from Refs. [15,17,30] in Table III, the bound T_{cc} ground state is found only in our present work and Refs. [15,17] where the hyperfine potential is of the Yukawa type. Therefore, one can reach a conclusion that a Yukawa type hyperfine potential is necessary to accurately describe the short range interactions within the tetraquark system. The difference in the binding energy between Refs. [15,17] and our present work consists largely in the difference in the detailed form of the hyperfine potentials used in each model.

To investigate the effect of the forms of hyperfine potential on the binding energy and size of the T_{cc} configuration, we compare the contributions from the Yukawa and Gaussian types of potentials.

A. Detailed analysis of hyperfine potential

In the T_{cc} configuration, an important contribution to the binding comes from the hyperfine potential, which can be isolated as follows.

$$B^{\mathrm{Hyp}} \equiv H^{\mathrm{Hyp}}_{\mathrm{Tetraquark}} - H^{\mathrm{Hyp}}_{\mathrm{Meson1}} - H^{\mathrm{Hyp}}_{\mathrm{Meson2}}, \tag{12}$$

where $H^{\mathrm{Hyp}}_{\mathrm{Tetraquark}} \equiv \sum_{i<j}^{4} V^{CS}(i,j)$ and $H^{\mathrm{Hyp}}_{\mathrm{Meson}}$'s are the hyperfine part of the Hamiltonian calculated with the corresponding total wave functions for the tetraquark and the mesons, respectively.

We first analyze the contribution from the hyperfine potential of the D or D^* meson. Figure 1 compares the spatial functional form of the Yukawa and Gaussian type potentials, which indicates that the Yukawa type potential is stronger than the Gaussian type in the vicinity of the origin. However, as shown in Table IV, the contributions from the hyperfine potential for the threshold are the opposite of what one might expect. This is due to two factors. First, for both types of potential, the peak of the probability density of the D meson is at around 0.3 fm, as shown in Fig. 2. The probability density of the D^* shows almost the same as that of the D and the peak is at around 0.35 fm. Furthermore, the peak value of the Gaussian type is higher than that of the Yukawa type. Second, in this region, the spatial functional form of the Gaussian type for the $\bar{u}c$ pair is stronger than that of the Yukawa type, as shown in Fig. 1.

Besides, Fig. 3 shows that the size of the D or D^* meson is inversely proportional to the constituent quark masses. If the constituent quark masses in the Gaussian type are fitted to be lower than those used in Ref. [30], this leads to a

TABLE III. Masses and binding energies (B_T) of the tetraquark states. B_T is defined as the difference between the tetraquark mass and the sum of the masses of the lowest threshold mesons in the model calculations: $B_T \equiv M_{\mathrm{Tetraquark}} - M_{\mathrm{meson\,1}} - M_{\mathrm{meson\,2}}$. The mass and binding energy of $T_{cc}(\bar{u}\,\bar{d}\,cc)$ reported by LHCb [1] are 3875 MeV and −0.273 MeV, respectively. The masses and binding energies B_T are given in MeV. The values in the parentheses are the variational parameters (in fm^{-2}), which give the ground state energies.

			Present work		Refs. [15,17]		Ref. [30]	
Type	$I(J^P)$	Thresholds	Mass	B_T	Mass	B_T	Mass	B_T
$\bar{u}\,\bar{d}\,bb$	$0(1^+)$	BB^*	10464(3.7, 19.6, 3.6)	−144	10507	−144	10517(3.9, 25.0, 3.8)	−145
$\bar{u}\,\bar{d}\,cc$	$0(1^+)$	DD^*	3872(2.4, 4.0, 4.4)	−2	3899	−7	3873(2.6, 4.6, 4.6)	+13
$\bar{u}\,\bar{d}\,cb$	$0(1^+)$	DB^*	7179(2.7, 6.3, 4.8)	−18	⋯	⋯	7212(3.1, 8.0, 5.0)	−3

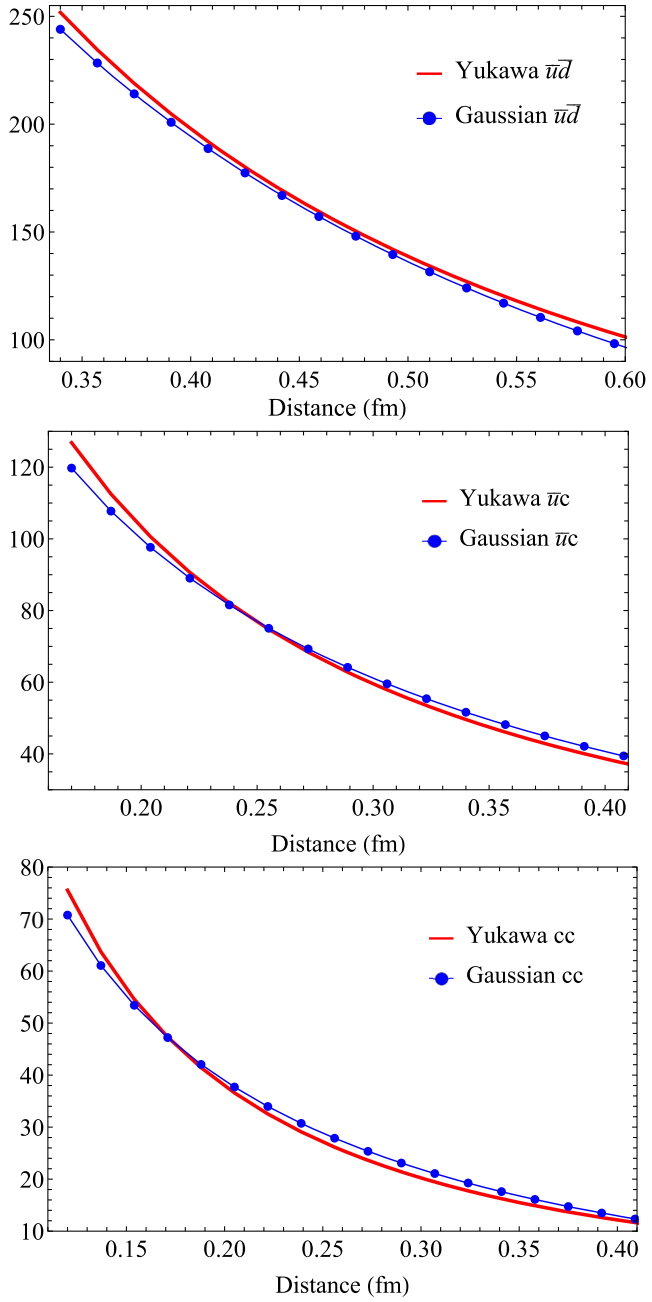

FIG. 1. Spatial forms of hyperfine potentials for the $\bar{u}\,\bar{d}$, $\bar{u}c$, and cc quark pairs. The red and blue lines represent that of the hyperfine potential used in this work and in Ref. [30], respectively. The Yukawa type is stronger in all range for the $\bar{u}\,\bar{d}$ pair, while the Gaussian type is slightly stronger in the range of around 0.25–0.6 fm for the $\bar{u}c$ pair and around 0.15–0.5 fm for the cc pair.

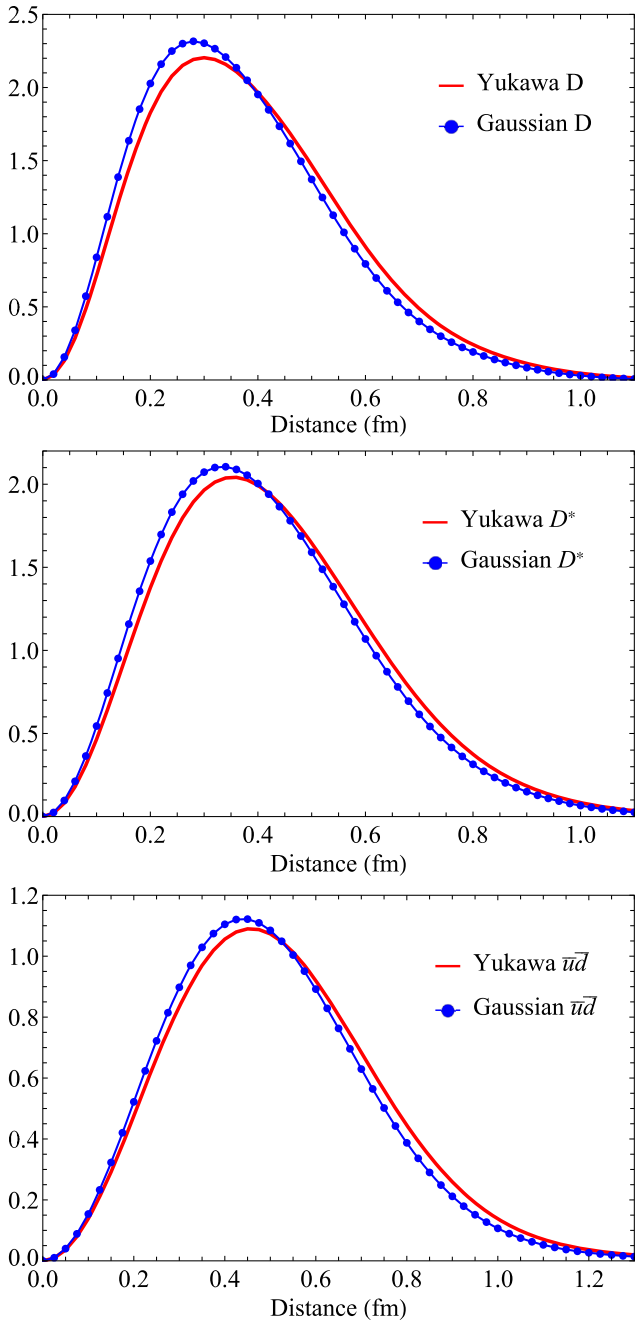

FIG. 2. The radial distribution of the probability density of the D, D^* mesons, and the $\bar{u}\,\bar{d}$ pair in the T_{cc} state. The $\bar{u}\,\bar{d}$ pair in the bottom panel is obtained in terms of the most dominant color $\mathbf{3}_{\bar{u}\,\bar{d}} \otimes \bar{\mathbf{3}}_{cc}$ state. The red and blue lines represent the distribution obtained from the hyperfine potential used in this work and in Ref. [30], respectively.

larger size for the D or D^* meson in the Gaussian type. For a proper analysis, we scale the horizontal axis with the same rate of mass change for each constituent quark. It is also possible to understand a similar behavior of T_{cc} through the dependence of the relative size of T_{cc} on the constituent quark masses, as shown in Fig. 3.

We now analyze the contributions from the hyperfine potential for each quark pair in T_{cc} given in Table IV. For the $\bar{u}\,\bar{d}$ pair in T_{cc}, Fig. 2 shows that the peak of the probability density for both types of potential is located at around 0.45 fm. For the $\bar{u}c$ and cc pairs, the peaks are slightly shifted from that of the $\bar{u}\,\bar{d}$ pair toward the origin:

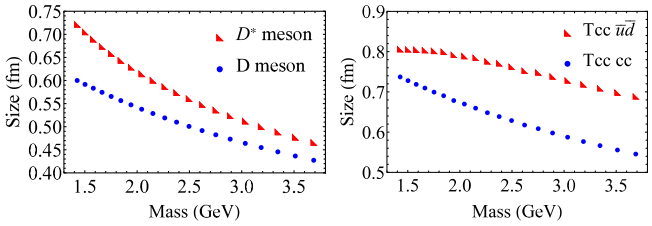

FIG. 3. Left panel shows the change in size of the D meson with increasing constituent quark masses using spatial bases up to the 5th quanta. Right panel shows the same for the $\bar{u}\,\bar{d}$ and cc pairs in T_{cc}, but using up to the 3rd quanta. The horizontal axis represents the sum of masses of the u and c quarks. The Gaussian type of hyperfine potential from Ref. [30] is used to obtain the figure.

the peak for the $\bar{u}c$ pair (cc pair) is at around 0.35 fm (0.3 fm). For the same reason as in the case of D or D^*, the contribution from the Gaussian type potential is found to be stronger than that of the Yukawa type for the $\bar{u}c$ and cc pairs as shown in Table IV. However, for the $\bar{u}\,\bar{d}$ pair, the strength of the Yukawa type hyperfine potential is above that of the Gaussian type in all ranges. Thus, for the $\bar{u}\,\bar{d}$ pair, we find that the relative contribution from the Gaussian and Yukawa types is opposite to those of the other pairs as shown in Table IV. Furthermore, the attraction from each type of hyperfine potential mainly comes from the $\bar{u}\,\bar{d}$ pair. Therefore, we find that the binding energy in Eq. (12) obtained from the Yukawa type potential is relatively attractive as shown in Table IV. These suggest that the $\bar{u}\,\bar{d}$ pair plays a crucial role in the hyperfine interaction in T_{cc}.

To get a better understanding of the size of T_{cc}, we examine the probability density. In Fig. 2, we find that the peak for the $\bar{u}\,\bar{d}$ pair of the Gaussian type is higher and closer to the origin than that of the Yukawa type. This trend is also observed for the $\bar{u}c$ and cc pairs. Therefore, all relative sizes of the quark pairs in T_{cc} for the Gaussian type are smaller than those for the Yukawa type, as shown in Table IV.

TABLE IV. Hyperfine potentials V^{CS} (in MeV) and relative length l (in fm). For T_{cc} configuration, we label the position of each quark as $\bar{u}(1)\bar{d}(2)c(3)c(4)$. The values for the quark pairs of (1, 4), (2, 3), and (2, 4) are the same as those of the (1, 3) pair due to symmetry. The subscripts Y and G represent the results obtained using the hyperfine potential in Eq. (3) and the Gaussian potential from Ref. [30], respectively. The values of B^{Hyp} are calculated by Eq. (12).

	T_{cc}				Threshold			
Type	(1, 2)	(1, 3)	(3, 4)	Total	D	D^*	Total	B^{Hyp}
V^{CS}_{Y}	−112	−16.8	5.0	−175	−120	32.5	−88	−87
l_{Y}	0.87	0.71	0.64		0.55	0.61		
V^{CS}_{G}	−109	−17.4	5.3	−173	−127	34.1	−93	−80
l_{G}	0.83	0.67	0.61		0.52	0.59		

In order to discuss the compactness of the tetraquark states, we calculate the ratio Δ_R between the root mean square (RMS) radii for the tetaquark and its threshold using the following formula defined as Eqs. (9) and (10) of Ref. [17]:

$$\Delta_R = \frac{\mathrm{RMS}_{4q}}{\mathrm{RMS}_{\mathrm{Meson}_1} + \mathrm{RMS}_{\mathrm{Meson}_2}}, \tag{13}$$

where $\mathrm{RMS}_{4q(\mathrm{Meson})}$ is the RMS radius for four-(two-) quark systems. In particular, the RMS radius of the tetraquark is defined as follows.

$$\mathrm{RMS}_{4q} = \sqrt{\frac{\sum_{i=1}^{4} m_i \langle (r_i - R_{CM})^2 \rangle}{\sum_{i=1}^{4} m_i}}, \tag{14}$$

where m_i is the mass of the ith quark and R_{CM} is the center of mass. As shown in Fig. 2, the mesons calculated using the Gaussian type hyperfine potential have smaller sizes compared to those calculated using the Yukawa type potential. This tendency is also reflected in the RMS radii of the threshold mesons presented in Table V and in the relative lengths of each quark pair for the tetraquark. Subsequently, we calculate the RMS radii of tetraquarks using the parameter set determined for each type of hyperfine potential. We then find that the difference of the RMS radius in the tetraquarks between the two types of potential becomes larger compared to the difference in the threshold mesons. Consequently, the RMS ratios Δ_R obtained by the Gaussian type potential are smaller compared to those of the Yukawa type potential.

On the other hand, according to the discussion in Ref. [17], a RMS ratio smaller than 1 would represent a compact configuration when the state is bound. The RMS ratios for the Yukawa type in Table V indicates that T_{bb} and T_{cb} are in compact configurations. Moreover, we infer that T_{cc} is also highly likely to be in a compact configuration.

Also, it would be interesting to compare our RMS radii with that of tetraquark structure composed of $udud$ flavors in a color **3** state in Ref. [31]. In that study, this tetraquark structure is considered as a part of d' dibaryon in a diquark-tetraquark cluster model. The results of Ref. [31] shows that

TABLE V. RMS radii in fm unit for the $T_{QQ'}$ states and corresponding lowest thresholds obtained with the Yukawa type of hyperfine potential in this work. The values in the parentheses represent the RMS radii obtained with the Gaussian type potential from Ref. [30]. The RMS radii and ratio Δ_R are calculated using Eq. (14).

Type	Tetraquark	Threshold	Δ_R
T_{bb}	0.209(0.198)	0.289(0.283)	0.723(0.700)
T_{cb}	0.294(0.271)	0.360(0.352)	0.817(0.770)
T_{cc}	0.400(0.382)	0.448(0.438)	0.893(0.872)

TABLE VI. The confinement V^C potential (in MeV) and the relative lengths l (in fm) for the $\bar{u}\bar{d}$ and cc pairs in T_{QQ}. The results are obtained using the Yukawa type potential in this work.

	T_{cc}		T_{bb}	
Type	$\bar{u}\bar{d}$	cc	$\bar{u}\bar{d}$	bb
$V^C(l)$	120(0.87)	48(0.64)	221(0.71)	−95(0.29)

the RMS radius varies depending on the radial form of the confinement potential. Specifically, for the colored $udud$ tetraquark, the size lies between 0.74 fm and 1.15 fm, demonstrating a considerable difference from our results for the tetraquarks consisting of two light antiquarks and two heavy quarks, as shown in Table V. Since the RMS radii in our model would also change as discussed in Ref. [31], it is worth investigating the effect of the radial form of confinement potential on the tetraquark structures in our study.

B. Principal differences between T_{cc} and T_{bb}

One of the most interesting findings is that the confinement potential of the $\bar{u}\bar{d}$ pair with $I = 0$ and cc (or bb) pair significantly contributes to the binding energy of the tetraquark. In particular, investigating the matrix element of $-\lambda_i^c\lambda_j^c$ is important because it affects the strength of the confinement potential. For both the light and heavy quark (Q) pairs, the value with respect to the most dominant color state, $\mathbf{3}_{\bar{u}\bar{d}} \otimes \bar{\mathbf{3}}_{QQ}$, is $\frac{8}{3}$. Thus, as shown in V_{ij}^C in Eq. (2), the linearizing potential gives repulsion while the Coulomb potential gives attraction in the confinement for both pairs.

For the light quark pair, the dominant part of the confinement potential comes from the linearizing potential in both T_{cc} and T_{bb} because their sizes are comparable to those of hadrons. However, the confinement potential in T_{bb} is considerably more repulsive than that in T_{cc}, as shown in Table VI, though the size of the light quark pair in T_{bb} is shorter than that of T_{cc}.

For the heavy quark pair, the dominant part still comes from the linearizing potential for the T_{cc} despite the small size of the cc pair. In contrast, for T_{bb}, it comes from the Coulomb potential because the size of heavy quark pair in T_{bb} shrinks much shorter than that in T_{cc}. Thus, the confinement potential for T_{cc} gives small repulsion while it gives significant attraction for T_{bb}. In addition to this, there is also hyperfine attraction for T_{bb}, which can be evaluated by Eq. (12) and is comparable to that of T_{cc}. Therefore, the ground state of T_{bb} is deeply bound as shown in Table III.

To understand the confinement contributions in Table VI, it is necessary to divide the probability distribution of the ground state in terms of each color state of the tetraquark as in Fig. 4. The values of $-\lambda_i^c\lambda_j^c$ in the confinement are changed by the probability distribution for the two color states when considering the whole of bases to calculate the Hamiltonian. In Fig. 4, the contribution from the color $\bar{\mathbf{6}}_{\bar{u}\bar{d}} \otimes \mathbf{6}_{QQ}$ state, where the matrix element for both the light and heavy quark pairs is $-\frac{4}{3}$, is negligible for T_{bb} but crucial for T_{cc}. Apart from the contribution of $\mathbf{3}_{\bar{u}\bar{d}} \otimes \bar{\mathbf{3}}_{QQ}$ to the values of $-\lambda_i^c\lambda_j^c$, the contribution of $\bar{\mathbf{6}}_{\bar{u}\bar{d}} \otimes \mathbf{6}_{QQ}$ to T_{cc} is relatively larger than that to T_{bb}. Therefore, the confinement potential involving the value of the matrix element for the $\bar{u}\bar{d}$ pair in T_{cc} decreases much compared to that in T_{bb}.

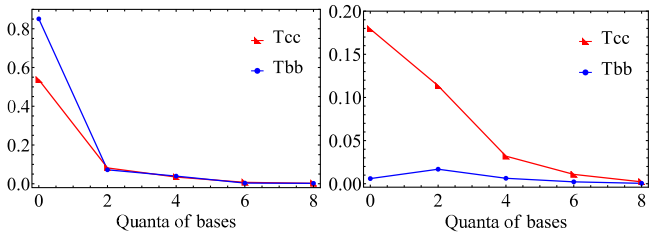

FIG. 4. Left(right) panel shows the probability distribution for each quanta of spatial wave functions for T_{cc} and T_{bb} in terms of the color $\mathbf{3}_{\bar{u}\bar{d}} \otimes \bar{\mathbf{3}}_{QQ}$ ($\bar{\mathbf{6}}_{\bar{u}\bar{d}} \otimes \mathbf{6}_{QQ}$) state.

Finally, we note that the significant contribution of $\bar{\mathbf{6}}_{\bar{u}\bar{d}} \otimes \mathbf{6}_{QQ}$ to the confinement in T_{cc} is an essential feature that only appears when all the wave functions are expanded by the complete set of harmonic oscillator bases. This effect does not appear in a simple quark model [22], which performs calculations using a single spatial basis.

IV. SUMMARY

We introduce the complete set of harmonic oscillator bases to obtain the exact solutions for the Hamiltonian of the tetraquarks. With our Yukawa type of hyperfine potential defined in Eq. (3), we successfully reproduce the experimental findings for the T_{cc} as can be found in Table III. In Sec. III, we compare and analyze our results, focusing on the difference between the two types of hyperfine potentials. Specifically, we calculate the radial distributions of the probability densities for the various quark pairs of the T_{cc} and the corresponding threshold configurations. Our results indicate that the Yukawa type hyperfine potential gives more attractive contribution to the T_{cc} than the Gaussian type, leading to a slightly bound T_{cc} state. Moreover, we suggest that T_{cc} is highly likely to be in a compact tetraquark structure, based on the ratio of the RMS radius. Finally, our analysis of the color interaction in the confinement potential shows that T_{bb} is much more deeply bound than T_{cc}.

ACKNOWLEDGMENTS

This work was supported by the Korea National Research Foundation under the Grant No. 2021R1A2C1009486(NRF).

[1] Roel Aaij *et al.* (LHCb Collaboration), Observation of an exotic narrow doubly charmed tetraquark, Nat. Phys. **18**, 751 (2022).

[2] S. K. Choi *et al.* (Belle Collaboration), Observation of a Narrow Charmonium-Like State in Exclusive $B^{\pm} \to K^{\pm}\pi^{+}\pi^{-}J/\psi$ Decays, Phys. Rev. Lett. **91**, 262001 (2003).

[3] Roel Aaij *et al.* (LHCb Collaboration), Observation of $J/\psi p$ Resonances Consistent with Pentaquark State in $\Lambda_b^0 \to J/\psi K^{-} p$ Decays, Phys. Rev. Lett. **115**, 072001 (2015).

[4] V. M. Abazov *et al.* (D0 Collaboration), Evidence for a $B_s^0\pi^{\pm}$ state, Phys. Rev. Lett. **117**, 022003 (2016).

[5] Roel Aaij *et al.* (LHCb Collaboration), Observation of a Narrow Pentaquark State, $P_c(4312)^{+}$, and of Two-Peak Structure of the $P_c(4450)^{+}$, Phys. Rev. Lett. **122**, 222001 (2019).

[6] J. l. Ballot and J. M. Richard, Four quark states in additive potentials, Phys. Lett. **123B**, 449 (1983).

[7] S. Zouzou, B. Silvestre-Brac, C. Gignoux, and J. M. Richard, Four quark bound states, Z. Phys. C **30**, 457 (1986).

[8] J. Carlson, L. Heller, and J. A. Tjon, Stability of dimesons, Phys. Rev. D **37**, 744 (1988).

[9] B. Silvestre-Brac and C. Semay, Systematics of $L = 0$ $q^2\bar{q}^2$ systems, Z. Phys. C **57**, 273 (1993).

[10] C. Semay and B. Silvestre-Brac, Diquonia and potential models, Z. Phys. C **61**, 271 (1994).

[11] S. Pepin, Fl. Stancu, M. Genovese, and J.-M. Richard, Tetraquarks with colour-blind forces in chiral quark models, Phys. Lett. B **393**, 119 (1997).

[12] Boris A. Gelman and Shmuel Nussinov, Does a narrow tetraquark $cc\bar{u}\,\bar{d}$ state exist?, Phys. Lett. B **551**, 296 (2003).

[13] J. Vijande, F. Fernandez, A. Valcarce, and B. Silvestre-Brac, Tetraquarks in a chiral constituent-quark model, Eur. Phys. J. A **19**, 383 (2004).

[14] D. Janc and M. Rosina, The $T_{cc} = DD^{*}$ molecular state, Few-Body Syst. **35**, 175 (2004).

[15] J. Vijande, E. Weissman, A. Valcarce, and N. Barnea, Are there compact heavy four-quark bound states?, Phys. Rev. D **76**, 094027 (2007).

[16] D. Ebert, R. N. Faustov, V. O. Galkin, and W. Lucha, Masses of tetraquarks with two heavy quarks in the relativistic quark model, Phys. Rev. D **76**, 114015 (2007).

[17] J. Vijande, A. Valcarce, and N. Barnea, Exotic meson-meson molecules and compact four–quark states, Phys. Rev. D **79**, 074010 (2009).

[18] Youchang Yang, Chengrong Deng, Jailun Ping, and T. Goldman, S-wave $QQ\bar{q}\,\bar{q}$ state in the constituent quark model, Phys. Rev. D **80**, 114023 (2009).

[19] Marek Karliner and Jonathan L. Rosner, Discovery of the Doubly Charmed Ξ_{cc} Baryon Implies a Stable $bb\bar{u}\,\bar{d}$ Tetraquark, Phys. Rev. Lett. **119**, 202001 (2017).

[20] Estia J. Eichten and Chris Quiqq, Heavy-Quark Symmetry Implies Stable Heavy Tetraquark Mesons $Q_iQ_j\bar{q}_k\bar{q}_l$, Phys. Rev. Lett. **119**, 202002 (2017).

[21] Si-Qiang Luo, Kan Chen, Xiang Liu, Yan-Rui Liu, and Shi-Lin Zhu, Exotic tetraquark states with the $qq\bar{Q}\,\bar{Q}$ configuration, Eur. Phys. J. C **77**, 709 (2017).

[22] Woosung Park, Sungsik Noh, and Su Houng Lee, Masses of the doubly heavy tetraquarks in a constituent quark model, Nucl. Phys. **A983**, 1 (2019).

[23] Ming-Zhu Liu, Tian-Wei Wu, Manuel Pavon Valderrama, Ju-Jun Xie, and Li-Sheng Geng, Heavy-quark spin and flavor symmetry partners of the $X(3872)$ revisited: What can we learn from the one boson exchange model?, Phys. Rev. D **99**, 094018 (2019).

[24] Chengrong Deng, Hong Chen, and Jialun Ping, Systematical investigation on the stability of doubly heavy tetraquark states, Eur. Phys. J. A **56**, 9 (2020).

[25] Gang Yang, Jialun Ping, and Jorge Segovia, Doubly-heavy tetraquarks, Phys. Rev. D **101**, 014001 (2020).

[26] Y. Tan, W. Lu, and J. Ping, Systematics of $QQ\bar{q}\,\bar{q}$ in a chiral constituent quark model, Eur. Phys. J. Plus **135**, 716 (2020).

[27] Qi-Fang Lü, Dian-Yong Chen, and Yu-Bing Dong, Masses of doubly heavy tetraquarks $T_{QQ'}$ in a relativized quark model, Phys. Rev. D **102**, 034012 (2020).

[28] Jian-Bo Cheng, Shi-Yuan Li, Yan-Rui Liu, Zong-Guo Si, and Tao Yao, Double-heavy tetraquark states with heavy diquark-antiquark symmetry, Chin. Phys. C **45**, 043102 (2021).

[29] Rudolf N. Faustov, Vladimir O. Galkin, and Elena M. Savchenko, Heavy tetraquarks in the relativistic quark model, Universe **7**, 94 (2021).

[30] Sungsik Noh, Woosung Park, and Su Houng Lee, Doubly heavy tetraquarks, $qq'\bar{Q}\,\bar{Q}'$, in a nonrelativistic quark model with a complete set of harmonic oscillator bases, Phys. Rev. D **103**, 114009 (2021).

[31] A. J. Buchmann, G. Wagner, and A. Faessler, The d' dibaryon in a colored cluster model, Phys. Rev. C **57**, 3340 (1998).